Published May 27, 2014

Special Section: Principle of Effective Stress

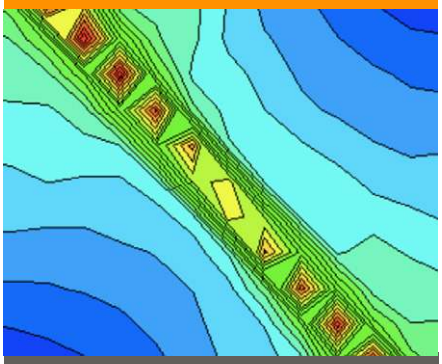

We develop a coupled solid deformation–fluid flow finite element model for unsaturated porous media with spatially varying density and degree of saturation. We use the model to investigate localized deformation in the form of a persistent shear band in unsaturated soil with random heterogeneity.

Finite Deformation and Fluid Flow in Unsaturated Soils with Random Heterogeneity

Xiaoyu Song and Ronaldo I. Borja*

The first law of thermodynamics suggests an energy-conjugate relationship among degree of saturation, suction stress, and density of an unsaturated porous material. Experimental evidence affirms that this constitutive relationship exists and that the water retention curves are dependent on the specific volume or density of the material. This constitutive feature must be incorporated into the mathematical formulation of boundary-value problems involving finite deformation. We present a fully coupled hydromechanical formulation in the finite deformation range that incorporates the variation of degree of saturation with the Kirchhoff suction stress and the Jacobian determinant of the solid-phase motion. A numerical simulation of solid deformation–fluid flow in unsaturated soil with randomly distributed density and degree of saturation demonstrates an intricate but well-established coupling of the hydromechanical processes. As deformation localizes into a persistent shear band, we show that bifurcation of the hydromechanical response manifests itself not only in the form of a softening behavior but also through bifurcation of the state paths on the water-retention surface.

The water retention curve, also called the soil-moisture characteristic curve, is a relationship between a soil's water content and water potential or between a soil's degree of saturation and the suction stress (Lu and Likos, 2004). It is used to predict the soil water storage in the mass balance equation, as well as to close the statement of the initial boundary-value problem for coupled solid deformation–fluid flow (Borja, 2004; Borja et al., 2012a, 2012b, 2013b; Buscarnera and Nova, 2011; Buscarnera and di Prisco, 2011, 2012; Diamantopoulos and Durner, 2012; Ehlers et al., 2011; Garcia et al., 2011; Goumiri et al., 2012; Guillon et al., 2012; Le et al., 2012; Lloret-Cabot et al., 2013; Mousavi Nezhad et al., 2011; Oostrom et al., 2012; Sun and Sun, 2012; Uzuoka and Borja, 2012; Zha et al., 2013). During the past few decades, the water retention curve for soils has been widely studied and is considered to be a fairly accurate representation of the water storage property under isothermal conditions, small deformation, monotonic loading, and even cyclic loading (Barquin-Valle et al., 2011; Hassanizadeh et al., 2002; Horta et al., 2013; Manzanal et al., 2011; Mohammadi and Vanclooster, 2011; Tamagnini, 2004; Zhang, 2011).

In has long been recognized that the water retention curve for unsaturated soils is a function of the density of the soil (Arairo et al., 2013; Miller et al., 2002; Sugii et al., 2002; Tarantino and Tombolato, 2005) as well as temperature (Arson and Gatmiri, 2012; Dumont et al., 2011; Mašín and Khalili, 2012; Imbert et al., 2005; Romero et al., 2001; Salager et al., 2006, 2011; Tang, 2005). For isothermal conditions, this means that the water retention curve must be defined for a given density and that, for soils undergoing finite volume changes, the water retention law must contain a third variable, namely, either density, porosity, specific volume, or any suitable measure of porosity changes in the soil. This is fulfilled by a more generalized water retention surface where one variable, say, the degree of saturation, may be interpreted as a function of two remaining independent variables, namely, the suction stress and specific volume. Such a constitutive relationship

Dep. of Civil and Environmental Engineering, Stanford University, Stanford, CA 94305. *Corresponding author (borja@stanford.edu).

Vadose Zone J.
doi:10.2136/vzj2013.07.0131
Received 16 July 2013.

is supported by continuum principles of thermodynamics (Borja 2004, 2006; Nikooee et al., 2013; Nuth and Laloui, 2008) and has already been established experimentally for different types of soil (Gallipoli et al., 2003b; Salager et al., 2010).

The solution of an initial boundary-value problem must accommodate governing conservation and constitutive laws, along with relevant boundary and initial conditions. Closed-form analytical solutions are available for unsaturated flow in one dimension (Ashayeri et al., 2011; Shan et al., 2012; Wu et al., 2012). However, they are severely handicapped by numerous simplifying assumptions, making them unsuitable for general-purpose problems. Furthermore, because of their limited kinematics, they cannot capture localized deformation phenomena. In this work, we adopted a mixed finite element formulation combined with mixture theory in a fully coupled hydromechanical framework. The formulation can accommodate some intricate aspects of hydromechanical processes, such as material and geometric nonlinearities as well as material heterogeneities at the mesoscopic scale, more naturally than can other equally robust methods, such as the meshless method (Khoshghalb and Khalili, 2012). *Mesoscopic* scale is a common term used to quantify the spatial variations of density, degree of saturation, and other continuum variables within a macroscopic element without the need to consider the complexities of the grain-scale processes (Andrade and Borja, 2006; Borja and Andrade, 2006; Borja et al., 2013a, 2013b; Mousavi Nezhad et al., 2011, 2013; Rechenmacher et al., 2011).

A finite deformation formulation is especially suited for a problem with an evolving solid matrix configuration in general and an evolving porosity in particular. Whereas the infinitesimal formulation can also be used to a certain extent, it is not as natural and consistent; it assumes that the solid displacements are small and so the solid matrix configuration is essentially unchanged. However, updating the porosity changes the solid matrix configuration, which is conceptually inconsistent with the idea behind the infinitesimal formulation. On the other hand, a finite deformation formulation naturally accommodates an evolving configuration characteristic of a deformable solid matrix. Finite volume changes are accommodated naturally by the so-called Jacobian determinant J, which represents the evolution of a differential volume in a solid matrix.

The specific problem simulated in this study was the hydromechanical response of a rectangular sample of unsaturated sand with imposed heterogeneities in density and degree of saturation. We considered both material and geometric nonlinearities—specifically, finite deformation including finite volume changes that could significantly impact the position of the field variables on the water retention surface. We used the first law of thermodynamics to identify energy-conjugate pairings of the constitutive variables, as well as to define a so-called effective, or constitutive, stress in both the infinitesimal and finite deformation regimes (Borja, 2004, 2006; Hassanizadeh and Gray, 1993; Houlsby, 1997). The sample is deformed until the hydromechanical response bifurcates into a deformation band. We show that bifurcation manifests itself not only through a localized deformation pattern but also through the hydromechanical movement of the field variables on the water retention surface.

Thermodynamic Basis

Our point of departure is the first law of thermodynamics for a mixture of solid, water, and air, which serves as the origin of the effective stress equation and the motivation for pairing different constitutive variables. Let ϕ^s, ϕ^w, and ϕ^a denote the respective volume fractions of solid, water, and air in the mixture, respectively, which satisfy the closure condition

$$1=\phi^s+\phi^w+\phi^a \qquad [1]$$

Further, let ρ_s, ρ_w, and ρ_a denote the intrinsic mass densities of solid, water, and air, respectively, defined as the mass of the constituent per unit volume of the constituent. The corresponding partial mass densities are $\rho^s=\phi^s\rho_s$, $\rho^w=\phi^w\rho_w$, and $\rho^a=\phi^a\rho_a$ defined as the mass of the constituent per unit volume of the mixture. The total mass density ρ of the mixture is then given by

$$\rho=\rho^s+\rho^w+\rho^a \qquad [2]$$

We also recall the partial Cauchy stress tensors $\boldsymbol{\sigma}^s$, $\boldsymbol{\sigma}^w$, and $\boldsymbol{\sigma}^a$ for solid, water, and air, respectively, which satisfy the closure condition

$$\boldsymbol{\sigma}=\boldsymbol{\sigma}^s+\boldsymbol{\sigma}^w+\boldsymbol{\sigma}^a \qquad [3]$$

where $\boldsymbol{\sigma}$ is the total Cauchy stress tensor.

The first law of thermodynamics applied to a mixture of solid, water, and air states that the rate of increase in the total energy (internal plus kinetic) of any arbitrary volume of the mixture is equal to the rate of work done on the mixture plus the rate of increase in heat energy. If there is no mass exchange between the species, the rate of change in internal energy per unit total volume of the mixture is given by

$$\rho\dot{\bar{e}}=\boldsymbol{\sigma}^s:\mathbf{d}+\sum_{\alpha=w,a}\boldsymbol{\sigma}^\alpha:\mathbf{d}_\alpha+r-\nabla\cdot\mathbf{q} \qquad [4]$$

where $\rho\dot{\bar{e}}$ is the rate of change in internal energy per unit total mass of the mixture, r is the heat supply per unit volume of the mixture, $\mathbf{q}$ is the heat flux vector, $\mathbf{d}$ is the rate of deformation tensor for the solid matrix, and $\mathbf{d}_w$ and $\mathbf{d}_a$ are the rate of deformation tensors for water and air, respectively. Assuming that $\boldsymbol{\sigma}^w$ and $\boldsymbol{\sigma}^a$ are isotropic tensors, we can write

$$\boldsymbol{\sigma}^w=-\phi^w p_w\mathbf{1},\quad \boldsymbol{\sigma}^a=-\phi^a p_a\mathbf{1} \qquad [5]$$

where p_w and p_a are the intrinsic pore water and pore air pressures, respectively, defined as the force in the fluid per unit area of that fluid.

Equation [4] can be written in the following alternative form following the developments presented by Borja (2006):

$$\rho\dot{\bar{e}} = \boldsymbol{\sigma}' : \mathbf{d} + \sum_{\alpha=w,a}\left[\frac{1}{\rho_\alpha}\nabla\cdot\left(\phi^\alpha\rho_\alpha\tilde{\upsilon}_\alpha\right) - \phi^\alpha\nabla\cdot\tilde{\upsilon}_\alpha\right]p_\alpha - s\left(1-\phi^s\right)\dot{S}_r + \sum_{\alpha=w,a}\left(\phi^\alpha\frac{\dot{p}_\alpha}{K_\alpha}\right)p_\alpha + r - \nabla\cdot\mathbf{q} \quad [6]$$

where $\tilde{\upsilon}_w$ and $\tilde{\upsilon}_a$ are the relative velocities of water and air, respectively, with respect to the solid, K_w and K_a are the elastic bulk moduli for water and air, respectively, S_r is the degree of saturation, and $s = p_a - p_w$ is the suction stress.

The first term on the right-hand side of Eq. [6] identifies the pairing between the effective Cauchy stress tensor $\boldsymbol{\sigma}'$ and the rate of deformation tensor $\mathbf{d}$ for the solid matrix. This motivates the development of a constitutive law for the solid matrix in terms of the effective Cauchy stress $\boldsymbol{\sigma}'$, which takes the form (Borja, 2006)

$$\boldsymbol{\sigma}' = \boldsymbol{\sigma} + \beta\bar{p}\mathbf{1}, \quad \bar{p} = S_r p_w + \left(1-S_r\right)p_a \quad [7]$$

where β is the Biot coefficient. The effective stress equation stated above approaches the Schrefler (1984) stress in the limit $\beta = 1$. Other schools of thought have led to the development of a slightly different expression for the effective stress (see Khalili et al., 2004).

The second term on the right-hand side of Eq. [6] identifies the pairing between the intrinsic pressure p_a and the relative velocity $\tilde{\upsilon}_\alpha$ and motivates the use of Darcy's law for the flow of water and air relative to the solid. The third term identifies the conjugate pairing among the suction stress s, porosity $n = 1 - \phi^s$, and degree of saturation S_r, which motivates the water retention surface of the form

$$S_r = S_r\left(s, 1-\phi^s\right) \quad [8]$$

The fourth term represents the mechanical powers of the intrinsic pore water and pore air pressures in volumetrically deforming the water and air, respectively. If we assume that water is incompressible and the pore air remains passive (i.e., $p_a = 0$), then these terms will drop out of the energy balance equation. Finally, the last two terms are non-mechanical powers associated with heat.

Without loss of generality, we shall make the simplifying assumptions of incompressible water and passive air, as well as $\beta = 1$. The expression for the rate of change of internal energy then becomes

$$\rho\dot{\bar{e}} = \boldsymbol{\sigma}' : \mathbf{d} + \left\langle p_w, \tilde{\upsilon}_w\right\rangle - s\left(1-\phi^s\right)\dot{S}_r + r - \nabla\cdot\mathbf{q} \quad [9]$$

where the symbol $\langle\cdot,\cdot\rangle$ denotes an energy-conjugate pairing. Now, let $\mathbf{F}$ denote the deformation gradient for the solid-phase motion, and $J = \det(\mathbf{F})$ the corresponding Jacobian determinant. Multiplying both sides of the expression for the internal energy by J, and assuming a passive air condition, we get

$$\rho_0\dot{\bar{e}} = \boldsymbol{\tau}' : \mathbf{d} + \left\langle \vartheta_w, \tilde{\upsilon}_w\right\rangle + \vartheta_w\left(1-\phi^s\right)\dot{S}_r + R - \mathrm{DIV}(\mathbf{Q}) \quad [10]$$

where $\rho_0 = J\rho$ is the pull-back mass density of the mixture, $\boldsymbol{\tau}' = J\boldsymbol{\sigma}'$ is the effective Kirchhoff stress tensor, $\vartheta_w = Jp_w$, $R = Jr$, and $\mathbf{Q} = J\mathbf{F}^{-1}\mathbf{q}$ is the Piola identity. This yields the following effective stress equation in terms of the Kirchhoff stresses:

$$\boldsymbol{\tau}' = \boldsymbol{\tau} - S_r\vartheta_w\mathbf{1} \quad [11]$$

where $\boldsymbol{\tau} = J\boldsymbol{\sigma}$. In terms of the first Piola–Kirchhoff stress tensors, the effective stress equation takes the form

$$\mathbf{P}' = \mathbf{P} - S_r\vartheta_w\mathbf{F}^{-1} \quad [12]$$

where $\mathbf{P}' = \mathbf{F}^{-1}\boldsymbol{\tau}'$ and $\mathbf{P} = \mathbf{F}^{-1}\boldsymbol{\tau}$. Note that the Piola transform of the Kronecker delta is not an isotropic tensor.

Constitutive Assumptions

Assuming a passive air condition, conservation laws include the balance of linear momentum for the solid–water–air mixture and the balance of mass for the solid and water. A complete formulation of the initial boundary-value problem may be found in Borja et al. (2013a) for infinitesimal deformation and Song and Borja (2014) for finite deformation. Motivated by the discussions above, we complete the formulation of the initial boundary-value problem by providing specific constitutive relationships between the effective Kirchhoff stress and deformation of the solid matrix, the water retention properties of the soil, and a modified Darcy's law accounting for the deformation of the solid matrix.

Multiplicative Plasticity

The framework for the mechanical response of the soil is based on multiplicative decomposition of the deformation gradient. This framework is relatively mature, particularly for isotropic plasticity models where the product formula algorithm is readily available (Simo, 1992; Borja and Alarcón, 1995). A three-invariant constitutive model for unsaturated sand was first presented by Borja et al. (2013b) for infinitesimal plasticity. Song and Borja (2014) presented an extension of this model to the finite deformation regime. The elastic deformation of the soil is determined from a stored energy function $\Psi = \Psi(\mathbf{b}^e)$, where $\mathbf{b}^e$ is the left Cauchy–Green deformation tensor. Through a spectral decomposition of $\mathbf{b}^e$, one can choose, as the independent variables of this function, the volumetric and deviatoric invariants, ε_v^e and ε_v^s, respectively, of the

elastic logarithmic stretches. The effective Kirchhoff stress tensor $\boldsymbol{\tau}'$ is then obtained from the hyperelastic constitutive equation

$$\boldsymbol{\tau}' = 2\frac{\partial \Psi}{\partial \mathbf{b}^e}\mathbf{b}^e \qquad [13]$$

To characterize the plastic deformation of the soil, we need to define three components of a plasticity model, namely, a yield surface, a hardening law, and a flow rule. The yield surface depends on all three invariants of the effective Kirchhoff stress tensor:

$$p = \frac{1}{3}\mathrm{tr}(\boldsymbol{\tau}'), \quad q = \sqrt{\frac{3}{2}}\|\boldsymbol{\xi}\|, \quad \cos 3\theta = \sqrt{6}\frac{\mathrm{tr}(\boldsymbol{\xi}^3)}{\chi^3} \qquad [14]$$

where $\boldsymbol{\xi} = \boldsymbol{\tau}' - p\mathbf{1}$ is the deviatoric component of the effective Kirchhoff stress tensor $\boldsymbol{\tau}'$, and $\chi^2 = \mathrm{tr}(\boldsymbol{\xi}^2)$. The quantity p is called the *mean normal stress* and has a negative value throughout; θ is Lode's angle, whose value ranges from $0 \le \theta \le \pi/3$ (Borja 2013). The specific yield criterion is given by

$$F = \varsigma q + \eta p \le 0 \qquad [15]$$

where ς is a scaling function defined by Borja et al. (2013b). Lode's angle θ represents the effect of the third stress invariant modifying the shape of the yield surface on a deviatoric plane and η is defined as a function of the slope of the critical state line M, the curvature of the yield surface N on the hydrostatic axis, mean normal stress p, and image stress p_i (Borja et al., 2013b). Figure 1 shows a three-dimensional representation of the three-invariant yield surface in principal effective Kirchhoff stress space.

To simplify the formulation, we assume the associative flow rule and express the symmetric part of the plastic velocity gradient as

$$\mathbf{d}^p = \dot{\lambda}\frac{\partial F}{\partial \boldsymbol{\tau}'} \qquad [16]$$

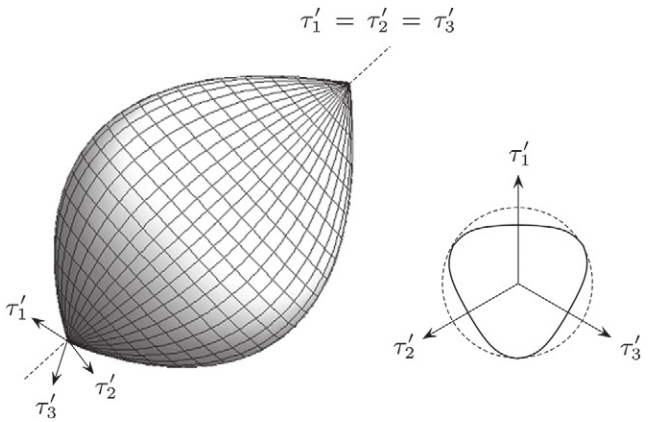

Fig. 1. Three-invariant yield surface in principal effective Kirchhoff stress space, where τ' is the effective Kirchhoff stress tensor.

where $\dot{\lambda}$ is the consistency parameter.

To complete the plasticity model, we need to define a hardening law that accommodates the effect of a spatially varying density. For the dry sand case, the hardening law is a function of deviatoric plastic strain that allows the proper qualitative capture of key features in both loose and dense sands (Jefferies, 1993; Borja and Andrade, 2006; Andrade and Borja, 2006, 2007; Borja et al., 2013a). In a critical-state isotropic model, preconsolidation pressure is a measure of the size of the yield surface in the fully saturated state. For isotropic plasticity models, the preconsolidation pressure characterizes the distance from the origin of the stress space to the intersection of the compression cap with the hydrostatic axis. Borja et al. (2013b) modified this hardening law to account for the partially saturated sand by enhancing the preconsolidation pressure with a so-called bonding variable ξ (Gallipoli et al., 2003a; Borja, 2004; Borja et al., 2013b):

$$\overline{p}_c = -\exp[a(\xi)](-p_c)^{b(\xi)} \qquad [17]$$

where $\overline{p}_c$ is the preconsolidation pressure in the fully saturated state, and $a(\xi)$ and $b(\xi)$ are functions of the so-called bonding variable ξ, which varies with Kirchhoff suction stress and degree of saturation. A returning mapping algorithm is used to numerically integrate the constitutive model (Song and Borja, 2014).

Water Retention Surface

A suitable water retention law is crucial for characterizing the effect of the degree of saturation on the hydromechanical properties of unsaturated porous media. Here, we adopt the water retention law proposed by Gallipoli et al. (2003b) in which the degree of saturation is a function of suction and porosity. Recalling that for the problem at hand, the Kirchhoff suction stress $-\vartheta_w > 0$ (see Hassanizadeh and Gray, 1993), whereas the porosity $1 - \phi^s$ is a linear function of the Jacobian determinant J of the solid-phase motion, we write

$$S_r = \left\{1 + \left[-a_1\left(\frac{J}{\phi_0^s} - 1\right)^{a_2}\vartheta_w\right]^n\right\}^{-m} \qquad [18]$$

where $\phi_0{}^s$ is the initial solid volume fraction and a_1, a_2, m, and n are material parameters. This soil-water retention law is a simplified extension of the soil-water retention curve presented by van Genuchten (1980) in that as $\vartheta_w \to 0$, $S_r \to 0$ and as $\vartheta_w \to -\infty$, $S_r \to 0$. However, this relationship can capture the effect of porosity on the degree of saturation. On the other hand, it does not take into account the hydraulic hysteresis on wetting and drying (Khalili and Zargarbashi, 2010). Gallipoli et al. (2003b) used this relationship to characterize the water retention behavior of a compacted Speswhite kaolin. Salager et al. (2010) conducted laboratory tests on clayey silty sand and also obtained a similar relationship,

although they only showed their results graphically without an explicit equation. Here, we apply a three-dimensional curving fitting technique on the experimental data presented by Salager et al. (2010) to arrive at the following coefficients for the water retention surface defined by Eq. [18]: $a_1 = 3.8038 \times 10^{-2}$, $a_2 = 3.4909$, $m = 6.3246 \times 10^{-1}$, and $n = 7.1771 \times 10^{-1}$ for the clayey silty sand. Figure 2 shows such a surface in the space defined by the degree of saturation S_r, suction stress $-\vartheta_w$, and specific volume v. We used this particular water retention model for the numerical simulations presented below.

Modified Darcy's Law

We apply the modified Darcy's law to express the superficial velocity $\overline{\upsilon}$ in the unsaturated state as

$$\overline{\upsilon} = -Jk_{rw}k_{sa}1\nabla\left(\frac{\vartheta_w}{\gamma_w} + z\right) \qquad [19]$$

where k_{rw} is the relative permeability of the wetting phase of water related to the soil-water retention curve, k_{sa} is the isotropic saturated hydraulic conductivity, γ_w is the unit weight of water, and z is the vertical coordinate. We use the Kozeny–Carman equation (Bear, 1972) to express the saturated permeability in the form

$$k_{sa} = \frac{\gamma_w}{\mu}\frac{D^2}{180}\frac{\left(J - \phi_0^s\right)^3}{J\left(\phi_0^s\right)^2} \qquad [20]$$

where μ is the dynamic viscosity of water, D is the effective diameter of the grains, J is the Jacobian determinant, and ϕ_0^s is the initial volume fraction of the solid grains. The relative permeability is a function of the degree of saturation through the van Genuchten (1980) equation:

$$k_{rw} = S_r^{1/2}\left[1 - \left(1 - S_r^{1/m}\right)^m\right]^2 \qquad [21]$$

where m is the same material constant used in Eq. [18]. The degree of saturation S_r is calculated from Eq. [18], so k_{rw} is now also a function of the suction stress and deformation of the solid matrix.

Numerical Simulations

We conducted numerical simulations of the vertical compression of a rectangular specimen of unsaturated sand deforming in plane strain. Drainage conditions were specified such that water could not escape or enter through the outer boundaries of the sample, but could flow internally within the sample, i.e., the flow was globally undrained but locally drained. Because the balance of air mass was not imposed explicitly, air was assumed to drain freely through the atmosphere. The two vertical faces of the sample were exposed to an external confining pressure σ_c, whereas the top and bottom horizontal faces were supported on rollers except for one corner of the specimen that was pinned to the support to prevent rigid-body translation. A downward vertical displacement $\delta = \delta(t)$ was then prescribed at the top supports to compress the sample. This experimental setup, depicted in Fig. 3, is a realistic representation of a displacement-driven plane strain testing of a sand sample supported on a smooth base (Borja et al., 2013a).

The boundary conditions described above favor the development of a homogeneous deformation, and so, it is necessary to introduce imperfections into the soil sample to trigger inhomogeneous deformation. In this example, imperfections were introduced into the soil sample in the form of spatially varying density and degree of saturation. Randomization of the density, or specific volume, in the specimen was achieved through a random function generator

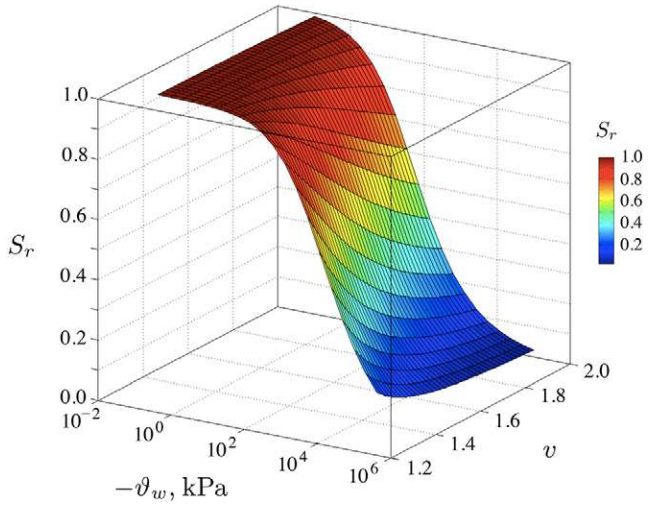

Fig. 2. Water retention surface for clayey silty sand as determined by the degree of saturation (S_r), Kirchhoff pore pressure (ϑ_w), and the specific volume (υ).

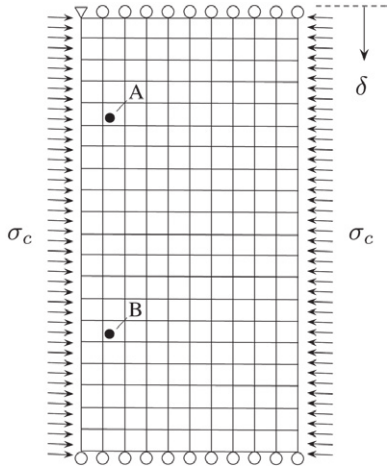

Fig. 3. Finite element mesh and boundary conditions, including the mean vertical compression (δ) and the confining pressure (σ_c). Soil sample is 5 by 10 cm deforming in plane strain. Material points A and B are Gauss points outside and inside the band, respectively.

with a probability distribution available in MATLAB. However, unlike in a previous study where inhomogeneities in density and degree of saturation were imposed independently (Borja et al., 2013a), the adoption of a water retention surface makes the suction, degree of saturation, and density interdependent on each other.

Initial conditions were established as follows. Uniform effective stresses were specified initially at the Gauss points, while uniform negative pore water pressures were specified initially at the pore pressure nodes. Because of the assumption of a passive air condition, a uniform suction equal to the negative of the pore water pressure was generated at the nodes, as well as throughout the entire problem domain including the Gauss points. A spatially varying specific volume was then specified at the Gauss points based on the random function generator. Because the degree of saturation depends on the suction stress and density, and because the suction stress was specified as being uniformly distributed throughout the sample, the spatial variation of the degree of saturation follows the same pattern as the spatial variation of specific volume. In general, the prescribed initial effective stresses and pore water pressures cannot be expected to be in static equilibrium with the externally applied confining pressures because the total stresses at the Gauss points also depend on the degree of saturation, which cannot be specified independently. Therefore, the first time step of the analysis, with a very small time interval Δt and no incremental compression, was used to *iteratively* find an equilibrium configuration. For purposes of analysis, the initial configuration where the Jacobian determinant J is set to unity was taken as the converged stress configuration after this first time step.

The soil sample was 5 cm wide by 10 cm tall and subjected to a confining stress of σ_c = 120 kPa on the two vertical faces (Fig. 3). The finite element mesh consisted of 861 solid nodes, 231 pore pressure nodes, and 200 isoperimetric quadrilateral elements with nine displacement nodes and four pore pressure nodes (Q9P4). This mixed element is convergent in the sense that it satisfies the Ladyženskaja–Babuška–Brezzi (LBB) stability condition (Brezzi, 1990) and has been used for similar finite deformation simulations by Li et al. (2004), Andrade and Borja (2007), and Uzuoka and Borja (2012). The confining stress σ_c was assumed constant throughout the simulation; however, because the configuration of the sample is changing due to finite deformation, the equivalent nodal forces generated by the confining pressure is configuration dependent. The contribution of the confining pressure to the algorithmic tangent operator is obtained by direct linearization of the equivalent nodal forces with respect to the configuration of the sample.

Table 1 summarizes the relevant material parameters for the sand constitutive model. The values of the parameters are similar to those used by Borja et al. (2013b). The specimen was compressed at the rate of 0.01 mm/s, Δt = 1 s, and the total number of increments = 310. We remark that the hydromechanical response is generally a function of the rate of compression due to the fluid flow occurring internally within the soil sample.

Table 1. Summary of material parameters for unsaturated sands (for physical meanings of these parameters, see Borja and Andrade, 2006; Andrade and Borja, 2006).

Symbol	Value	Parameter
$\tilde{\kappa}$	0.03	compressibility
p_0	−0.12 MPa	reference pressure
μ_0	16 MPa	shear modulus
M	1.1	critical state parameter
$\tilde{\lambda}$	0.1	compressibility parameter
N	0.4	yield surface parameter
β	1.0	nonassociative parameter
h	280	dimensionless hardening parameter
v_{c0}	1.85	reference specific volume
ρ	7/9	ellipticity
α	−3.5	limit dilatancy parameter

To generate a spatially varying initial specific volume in the specimen, we specified a range of [1.56, 1.61], a mean value of 1.58, a standard deviation of 0.009, and a normal distribution for this state variable. Figure 4 shows one realization of the specific volume. In generating this realization, we assumed that all nine Gauss points in a quadrilateral element have the same weight, so that only 200 random values would have to be generated (equal to the total number of finite elements). Furthermore, we specified an initial homogeneous suction stress of 20 kPa and an initial isotropic effective stress of −100 kPa (i.e., compressive). The corresponding range of values of the degree of saturation is $S_r \in [0.877, 0.896]$, with a mean value of 0.887. Figure 4 also shows the initial spatial variation of the degree of saturation within the soil sample. Note that the two contours follow the same trend because the suction stress is uniform. It is also possible to generate a different realization for

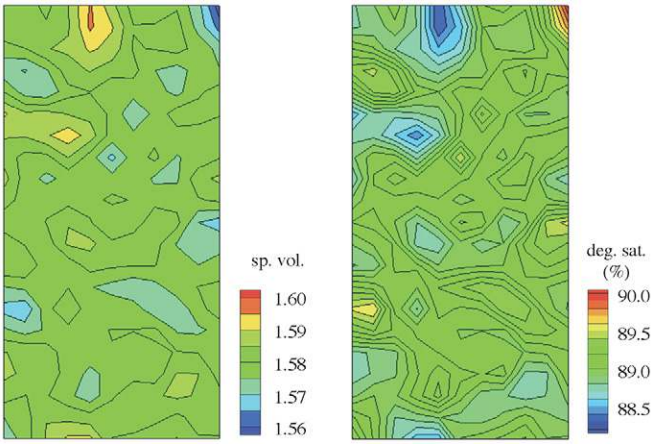

Fig. 4. Contours of initial specific volume (left) and initial degree of saturation (right). Note that the two contours follow the same trend for a uniform suction.

the degree of saturation if the suction stress is specified to follow its own random distribution.

Figure 5 shows the evolution of the second invariant of deviatoric strain within the sample, calculated from the principal logarithmic stretches of the deformation gradient **F** of the solid matrix. The deviatoric strains are initially homogeneous, but at a vertical compression of 2.6 mm, the sample begins to exhibit a tendency to form a shear band that propagates upward to the right. At a vertical compression of 3.1 mm, a persistent shear band is fully resolved (Borja, 2013). We should emphasize that the finite element mesh has no bias whatsoever; it is composed of symmetric quadrilateral elements with boundary conditions favoring the development of a homogeneous deformation pattern. The tendency of the solution to resolve a persistent shear band in this example is due solely to the heterogeneity in the deformation and fluid flow variables, as well as how they evolve with vertical compression.

Figure 6 depicts a more illuminating evolution of the fluid flow variables. The suction stress evolves from its initial uniform distribution to one that reflects the emerging persistent shear band, with mean values of around 3 kPa inside the shear band and 6 kPa outside the shear band at a vertical compression of 3.1 mm. Overall, the suction stress has reduced significantly from its initial uniform value of 20 kPa. Concurrently, the degree of saturation has evolved from its initial random distribution to one that also reflects the emerging shear band, with mean values of around 0.97 inside the shear band and 0.955 outside the shear band. This is a significant increase in the degree of saturation from its initial overall mean value of 0.887 at the beginning of the loading program. Because the water is not free to drain through the boundaries of the problem domain, we can conclude that the overall increase in degree of saturation inside the soil sample is due primarily to the compression of the air voids inside the sample. Moreover, we can expect that more air voids have compacted inside the shear band, where the degree of saturation is higher.

Indeed, the more pervasive compaction of the air voids inside the shear band is corroborated by the volumetric strain contours of Fig. 7. The volumetric strain in this case is the sum of the elastic and plastic natural logarithmic stretches, which is equal to the natural logarithm of the Jacobian determinant J (Borja, 2013, Chapter 6). The volumetric strains are all negative, implying that the sample has compacted everywhere, i.e., $J < 1$. However, compaction is more pervasive inside the shear band than outside, suggesting that the deformation band that forms is that of a compactive shear band (Borja and Aydin, 2004). At around this vertical compression, some material points inside the compactive shear band have undergone strain localization as the determinant of the drained acoustic tensor reverses in sign (Rudnicki and Rice, 1975). Note from the plot of the localization function that the material points outside the band remain stable in the sense that the localization function is nowhere close to zero. In a way, this is equivalent to the vertical compression being converted into localized deformation

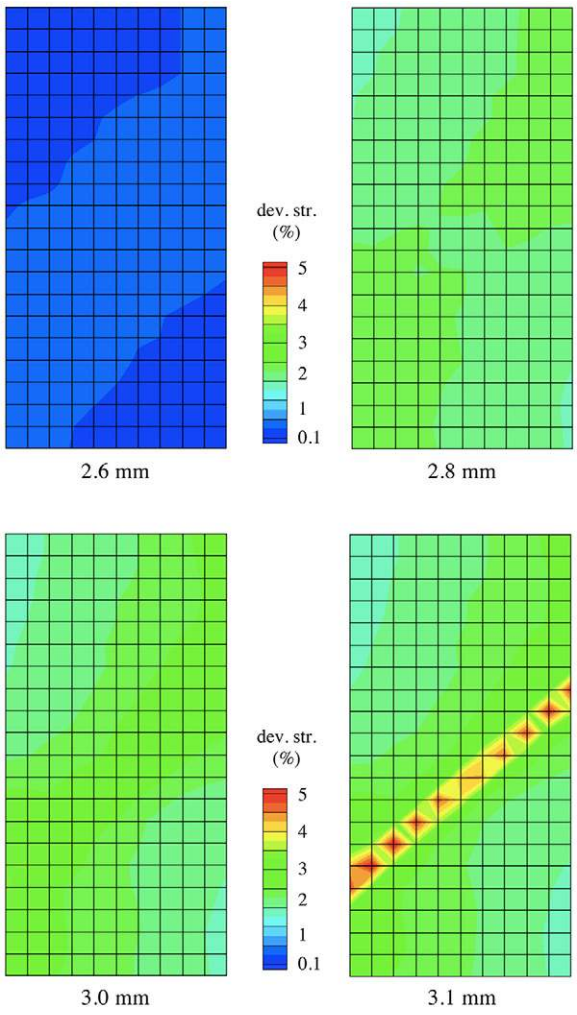

Fig. 5. Evolution of second invariant of deviatoric strain with vertical compression. Numbers in millimeters are vertical compression.

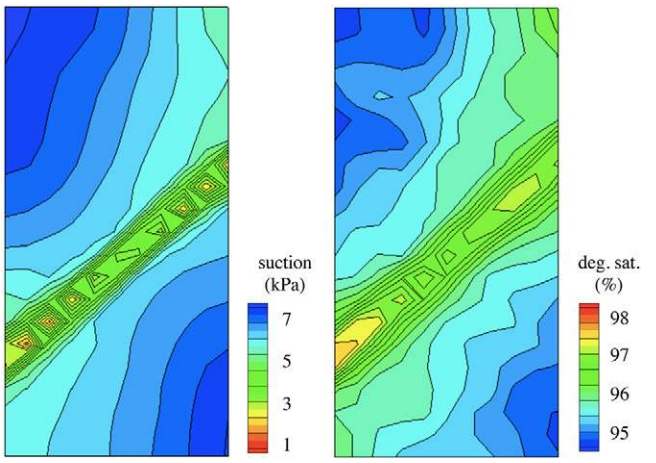

Fig. 6. Contours of Kirchhoff suction stress $\vartheta = -\vartheta_w$ (left) and degree of saturation S_r (right) at a vertical compression of 3.1 mm. Recall that the suction stress was initially uniformly distributed throughout the soil sample.

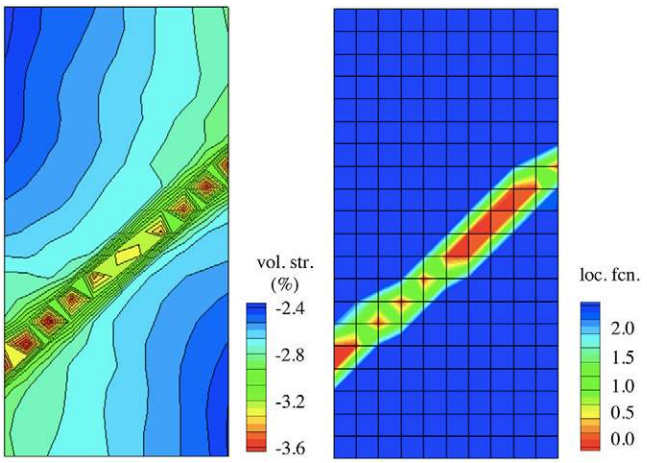

Fig. 7. Contours of volumetric strain (left) and normalized determinant of the localized function (right) at a vertical compression of 3.1 mm.

along the band, with the subdomain outside the band deforming essentially as a rigid body after the band has formed.

Figure 8 compares two load–compression curves, one for the heterogeneous sample under study and the other for an equivalent homogeneous sample with density and degree of saturation equal to the mean values of those of the heterogeneous sample. During the early part of loading, the two load–compression curves are nearly on top of one another. This is to be expected since the heterogeneous specimen is nearly homogeneous except for some small statistical variations in density and degree of saturation, as indicated in Fig. 4. As loading approaches the peak value, however, the two curves start to diverge slightly, with the heterogeneous soil sample exhibiting a slightly softer behavior and the homogeneous sample showing no sign of bifurcation. This result demonstrates that even relatively small imperfections can trigger strain localization. The first element to localize bifurcates at a vertical compression of around 2.9 mm, near the peak. Beyond this

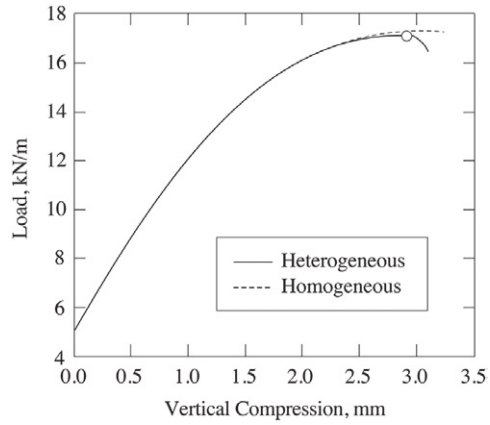

Fig. 8. Comparison of load–compression curves for heterogeneous and homogeneous soil samples. The homogeneous sample had a uniform density and degree of saturation equal to the mean values of the heterogeneous sample. The open circle shows the location of the first bifurcation point in the shear band.

bifurcation point, the heterogeneous sample exhibits a marked softening response; in contrast, the homogeneous sample continues to approach a plateau. Clearly, the homogeneous sample is unable to undergo strain localization because it lacks a trigger to such a mechanism. At a vertical compression of 3.1 mm, the persistent shear band has developed completely. This vertical compression occurs a little after the first bifurcation point but not too far beyond it for the solution to be afflicted significantly by mesh-dependency issues. In general, finite element enhancement techniques, such as the assumed enhanced strain and extended finite element methods, must be used to capture the evolution of the persistent shear band and circumvent the mesh-dependency issues associated with the loss of ellipticity well past the bifurcation point (Borja, 2013).

Figure 9 portrays an interesting comparison of two state paths on the water retention surface for two material points inside the soil sample, indicated in Fig. 1 and labeled as Gauss Point A, which is well outside the band, and Gauss Point B, which lies inside the band. The two Gauss points started out with nearly the same coordinates on the water retention surface, and their state paths are nearly the same during the early stage of compression. This is to be expected when the specific volume is specified to have a very narrow range within the sample and when its variation is only statistical in nature, as in this particular example. As Gauss Point B approaches the bifurcation point, its state path deviates ever so slightly from that of Gauss Point A. Right after bifurcation, however, as indicated by an open circle in Fig. 9, the state path for material Point B diverges significantly from that of Point A, whose state path remains nearly immobile. This is a remarkable finding in that it clearly shows that bifurcation of the field response can also

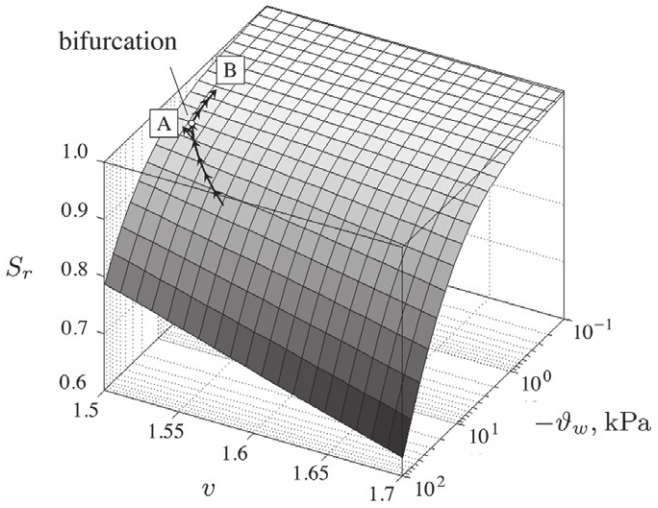

Fig. 9. Bifurcation on the water retention surface during plane strain compression of unsaturated sand; S_r is the degree of saturation, $-\vartheta_w$ is the Kirchhoff suction stress, and v is the specific volume. Gauss Point A is a material point outside the band, which has not bifurcated; Gauss Point B is a material point inside the band, which has bifurcated (see Fig. 3); the open circle indicates the bifurcation point for Gauss Point B.

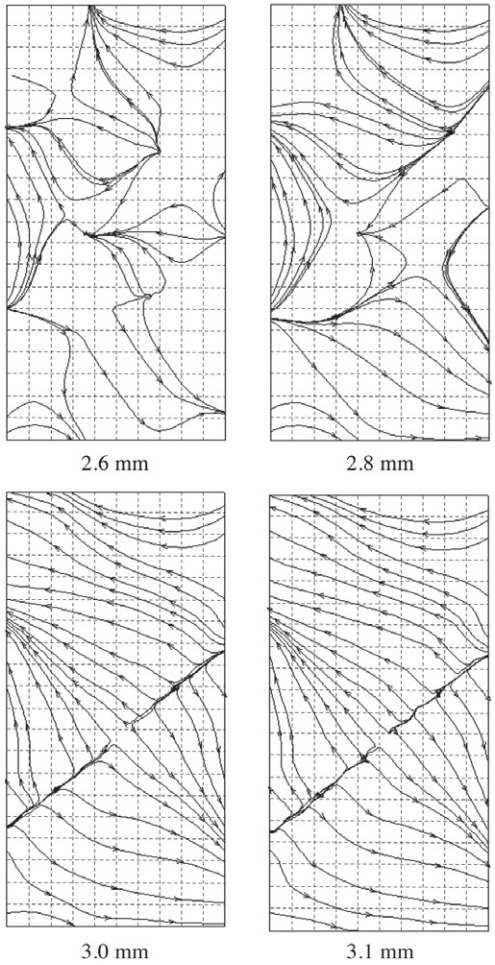

Fig. 10. Evolution of stream lines with vertical compression. Numbers in millimeters are vertical compression.

manifest itself on the water retention surface. As the strain localizes inside the band, more and more air voids are squeezed out until Gauss Point B reaches a nearly perfectly saturated state as manifested by the suction stress approaching zero while the specific volume remains steady at a nearly constant value, suggesting that deformation inside the band is close to the critical state. As the degree of saturation approaches 100% inside the band, the pressure gradient builds up and triggers fluid flow. This is demonstrated by the fluid flow patterns depicted in Fig. 10.

Figure 10 shows the evolution of stream lines with vertical compression. During the early part of compression (e.g., 2.6 mm), the flow lines are as random as the spatial variations of specific volume and degree of saturation, i.e., there is no distinct fluid flow pattern within the sample. As the vertical compression progresses (2.8 mm), the random distribution of fluid flow appears to evolve into a more recognizable pattern reflecting the developing compactive shear band. At a vertical compression of 3.0 mm, the shear band has become a source of fluid: the pore water pressure inside the band has developed to such a level where fluid is now expelled from the deformation band and away from it. This continues up to a vertical compression of 3.1 mm, when the persistent compactive shear band has fully developed. We remark once again that the boundaries of the problem domain are no-flow boundaries, i.e., fluid may not escape from or enter through the boundaries. Therefore, the fluid flow trajectories of Fig. 10 simply delineate general directions where the water is going to fill up the air voids that are continually squeezed out of the soil sample. Overall, the mass of the water contained in the problem domain as well as that of the solid are conserved.

Closure

The mechanisms for fluid flow and solid deformation in an unsaturated porous material are highly intricate and necessitate a fully coupled hydromechanical formulation. The continuum principle of thermodynamics for a mixture of solid–water–air is extremely useful for identifying so-called effective stress and the energy-conjugate pairings of the constitutive variables necessary for closing the statement of the underlying initial boundary-value problem. We have shown how the finite deformation and fluid flow mechanisms play out in the context of an unsaturated porous material with random distributions of density and degree of saturation. To our knowledge, this is the first time that a porosity-dependent water retention law has been fully integrated into the solution of an initial boundary-value problem in the finite deformation range. A water retention surface is fully consistent with the first law of thermodynamics and has been established experimentally for a variety of unsaturated, deformable soils. The proposed framework also sets the foundation for a more generalized hysteretic water retention law that accounts for incremental nonlinearity on wetting and drying.

Acknowledgments

Support for this work was provided by the U.S. National Science Foundation under Contract no. CMMI-0936421 to Stanford University and by Fonds zur Förderung der Wissenschaftlichen Forschung (FWF) of Austria under Project no. L656-N22 to Universität für Bodenkultur.

References

Andrade, J.E., and R.I. Borja. 2006. Capturing strain localization in dense sands with random density. Int. J. Numer. Methods Eng. 67:1531–1564. doi:10.1002/nme.1673

Andrade, J.E., and R.I. Borja. 2007. Modeling deformation banding in dense and loose fluid-saturated sands. Finite Elem. Anal. Des. 43:361–383. doi:10.1016/j.finel.2006.11.012

Arairo, W., F. Prunier, I. Djéran-Maigre, and F. Darve. 2013. A new insight into modelling the behavior of unsaturated soils. Int. J. Numer. Anal. Methods Geomech. 37:2629–2654.

Arson, C., and B. Gatmiri. 2012. Thermo-hydro-mechanical modeling of damage in unsaturated porous media: Theoretical framework and numerical study of the EDZ. Int. J. Numer. Anal. Methods Geomech. 36:272–306. doi:10.1002/nag.1005

Ashayeri, I., M. Kamalian, M.K. Jafari, and B. Gatmiri. 2011. Analytical 3D transient elastodynamic fundamental solution of unsaturated soils. Int. J. Numer. Anal. Methods Geomech. 35:1801–1829. doi:10.1002/nag.978

Barquin-Valle, L.P., K.W. Migliaccio, B. Schaffer, R. Munoz-Carpena, J.H. Crane, and Y. Li. 2011. Predicting soil water content using the "drained to equilibrium" concept. Vadose Zone J. 10:675–682. doi:10.2136/vzj2010.0073

Bear, J. 1972. Dynamics of fluids in porous media. American Elsevier Publ. Co., New York.

Borja, R.I. 2004. Cam-Clay plasticity: V. A mathematical framework for three-phase deformation and strain localization analyses of partially saturated porous media. Comput. Methods Appl. Mech. Eng. 193:5301–5338. doi:10.1016/j.cma.2003.12.067

Borja, R.I. 2006. On the mechanical energy and effective stress in saturated and unsaturated porous continua. Int. J. Solids Struct. 43:1764–1768. doi:10.1016/j.ijsolstr.2005.04.045

Borja, R.I. 2013. Plasticity: Modeling & computation. Springer-Verlag, Berlin.

Borja, R.I., and E. Alarcón. 1995. A mathematical framework for finite strain elastoplastic consolidation: 1. Balance laws, variational formulation, and linearization. Comput. Methods Appl. Mech. Eng. 122:145–171. doi:10.1016/0045-7825(94)00720-8

Borja, R.I., and J.E. Andrade. 2006. Critical state plasticity: VI. Meso-scale finite element simulation of strain localization in discrete granular materials. Comput. Methods Appl. Mech. Eng. 195:5115–5140. doi:10.1016/j.cma.2005.08.020

Borja, R.I., and A. Aydin. 2004. Computational modeling of deformation bands in granular media: I. Geological and mathematical framework. Comput. Methods Appl. Mech. Eng. 193:2667–2698. doi:10.1016/j.cma.2003.09.019

Borja, R.I., X. Liu, and J.A. White. 2012a. Multiphysics hillslope processes triggering landslides. Acta Geotech. 7:261–269. doi:10.1007/s11440-012-0175-6

Borja, R.I., X. Song, A.L. Rechenmacher, S. Abedi, and W. Wu. 2013a. Shear band in sand with spatially varying density. J. Mech. Phys. Solids 61:219–234. doi:10.1016/j.jmps.2012.07.008

Borja, R.I., X. Song, and W. Wu. 2013b. Cam-Clay plasticity, Part: VII. Triggering a shear band in variably saturated porous media. Comput. Methods Appl. Mech. Eng. 261–262:66–82. doi:10.1016/j.cma.2013.03.008

Borja, R.I., J.A. White, X. Liu, and W. Wu. 2012b. Factor of safety in a partially saturated slope inferred from hydro-mechanical continuum modeling. Int. J. Numer. Anal. Methods Geomech. 195:5115–5140.

Brezzi, F. 1990. A discourse on the stability conditions for mixed finite element formulations. Comput. Methods Appl. Mech. Eng. 82:27–57. doi:10.1016/0045-7825(90)90157-H

Buscarnera, G., and C. di Prisco. 2011. Stability criteria for unsaturated shallow slopes. Geotech. Lett. 1:85–90. doi:10.1680/geolett.11.00034

Buscarnera, G., and C. di Prisco. 2012. Discussing the definition of the second-order work for unsaturated soils. Int. J. Numer. Anal. Methods Geomech. 36:36–49. doi:10.1002/nag.991

Buscarnera, G., and R. Nova. 2011. Modelling instabilities in triaxial testing on unsaturated soil specimens. Int. J. Numer. Anal. Methods Geomech. 35:179–200. doi:10.1002/nag.832

Diamantopoulos, E., and W. Durner. 2012. Dynamic nonequilibrium of water flow in porous media: A review. Vadose Zone J. 11(3). doi:10.2136/vzj2011.0197

Dumont, M., S. Taibi, J. Fleureau, N. Abou-Bekr, and A. Saouab. 2011. A thermo-hydro-mechanical model for unsaturated soils based on the effective stress concept. Int. J. Numer. Anal. Methods Geomech. 35:1299–1317. doi:10.1002/nag.952

Ehlers, W., O. Avci, and B. Markert. 2011. Computation of slope movements initiated by rain-induced shear bands in small-scale tests and in situ. Vadose Zone J. 10:512–525. doi:10.2136/vzj2009.0156

Gallipoli, D., A. Gens, R. Sharma, and J. Vaunat. 2003a. An elasto-plastic model for unsaturated soil incorporating the effects of suction and degree of saturation on mechanical behavior. Geotechnique 53:123–135. doi:10.1680/geot.2003.53.1.123

Gallipoli, D., S. Wheeler, and M. Karstunen. 2003b. Modelling the variation of degree of saturation in a deformable unsaturated soil. Geotechnique 53:105–112. doi:10.1680/geot.2003.53.1.105

Garcia, E., F. Oka, and S. Kimoto. 2011. Numerical analysis of a one-dimensional infiltration problem in unsaturated soil by a seepage-deformation coupled method. Int. J. Numer. Anal. Methods Geomech. 35:544–568. doi:10.1002/nag.908

Goumiri, I.R., J.H. Prévost, and M. Preisig. 2012. The effect of capillary pressure on the saturation equation of two-phase flow in porous media. Int. J. Numer. Anal. Methods Geomech. 36:352–361. doi:10.1002/nag.1022

Guillon, T., R. Giot, A. Giraud, and G. Armand. 2012. Response of Callovo-Oxfordian claystone during drying tests: Unsaturated hydromechanical behavior. Acta Geotech. 7:313–332. doi:10.1007/s11440-012-0172-9

Horta, J., E. Rojas, M.L. Pérez-Rea, T. López, and J.B. Zaragoza. 2013. A random solid-porous model to simulate the retention curves of soils. Int. J. Numer. Anal. Methods Geomech. 37:932–944. doi:10.1002/nag.1133

Houlsby, G.T. 1997. The work input to an unsaturated granular material. Geotechnique 47:193–196. doi:10.1680/geot.1997.47.1.193

Hassanizadeh, S.M., M.A. Celia, and H.K. Dahle. 2002. Dynamic effect in the capillary pressure–saturation relations and its impacts on unsaturated flow. Vadose Zone J. 1:38–57. doi:10.2136/vzj2002.3800

Hassanizadeh, S.M., and W.G. Gray. 1993. Thermodynamic basis of capillary pressure in porous media. Water Resour. Res. 29:3389–3405. doi:10.1029/93WR01495

Imbert, C., E. Olchizky, T. Lassabatere, P. Dangla, and A. Courtois. 2005. Evaluation of a thermal criterion for an engineered barrier system. Eng. Geol. 81:269–283. doi:10.1016/j.enggeo.2005.06.019

Jefferies, M.G. 1993. Nor-Sand: A simple critical state model for sand. Geotechnique 43:91–103. doi:10.1680/geot.1993.43.1.91

Khalili, N., F. Geiser, and G.E. Blight. 2004. Effective stress in unsaturated soils: Review with new evidence. Int. J. Geomech. 4:115–126. doi:10.1061/(ASCE)1532-3641(2004)4:2(115)

Khalili, N., and S. Zargarbashi. 2010. Influence of hydraulic hysteresis on effective stress in unsaturated soils. Geotechnique 60:729–734. doi:10.1680/geot.09.T.009

Khoshghalb, A., and N. Khalili. 2012. A meshfree method for fully coupled analysis of flow and deformation in unsaturated porous media. Int. J. Numer. Anal. Methods Geomech. 37:716–743. doi:10.1002/nag.1120

Le, T.M.H., D. Gallipoli, M. Sanchez, and S.J. Wheeler. 2012. Stochastic analysis of unsaturated seepage through randomly heterogeneous earth embankments. Int. J. Numer. Anal. Methods Geomech. 36:1056–1076. doi:10.1002/nag.1047

Li, C., R.I. Borja, and R.A. Regueiro. 2004. Dynamics of porous media at finite strain. Comput. Methods Appl. Mech. Eng. 193:3837–3870. doi:10.1016/j.cma.2004.02.014

Lloret-Cabot, M., M. Sánchez, and S.J. Wheeler. 2013. Formulation of a three-dimensional constitutive model for unsaturated soils incorporating mechanical soil-water retention couplings. Int. J. Numer. Anal. Methods Geomech. 37:3008–3035. doi:10.1002/nag.2176

Lu, N., and W.J. Likos. 2004. Unsaturated soil mechanics. John Wiley & Sons, New York.

Manzanal, D., M. Pastor, and J.A.F. Merodo. 2011. Generalized plasticity state parameter-based model for saturated and unsaturated soils: II. Unsaturated soil modeling. Int. J. Numer. Anal. Methods Geomech. 35:1899–1917. doi:10.1002/nag.983

Mašín, D., and N. Khalili. 2012. A thermo-mechanical model for variably saturated soils based on hypoplasticity. Int. J. Numer. Anal. Methods Geomech. 36:1461–1485. doi:10.1002/nag.1058

Miller, C.J., N. Yesiller, K. Yaldo, and S. Merayyan. 2002. Impact of soil type and compaction conditions on soil water characteristic. J. Geotech. Geoenviron. Eng. 128:733–742. doi:10.1061/(ASCE)1090-0241(2002)128:9(733)

Mohammadi, M.H., and M. Vanclooster. 2011. Predicting the soil moisture characteristic curve from particle size distribution with a simple conceptual model. Vadose Zone J. 10:594–602. doi:10.2136/vzj2010.0080

Mousavi Nezhad, M., A.A. Javadi, A. Al-Tabbaa, and F. Abbasi. 2013. Numerical study of soil heterogeneity effects on contaminant transport in unsaturated soil (model development and validation). Int. J. Numer. Anal. Methods Geomech. 37:278–298. doi:10.1002/nag.1100

Mousavi Nezhad, M., A.A. Javahi, and F. Abbasi. 2011. Stochastic finite element modelling of water flow in variably saturated heterogeneous soils. Int. J. Numer. Anal. Methods Geomech. 35:1389–1408. doi:10.1002/nag.966

Nikooee, E., G. Habibagahi, S.M. Hassanizadeh, and A. Ghahramani. 2013. Effective stress in unsaturated soils: A thermodynamic approach based on the interfacial energy and hydromechanical coupling. Transp. Porous Media 96:369–396. doi:10.1007/s11242-012-0093-y

Nuth, M., and L. Laloui. 2008. Effective stress concept in unsaturated soils: Clarification and validation of a unified framework. Int. J. Numer. Anal. Methods Geomech. 32:771–801. doi:10.1002/nag.645

Oostrom, M., V.L. Freedman, T.W. Wietsma, J.H. Dane, and M.J. Truex. 2012. Effects of porous medium heterogeneity on vadose zone desiccation: Intermediate-scale laboratory experiments and simulations. Vadose Zone J. 11(4). doi:10.2136/vzj2011.0168

Rechenmacher, A.L., S. Abedi, O. Chupin, and A.D. Orlando. 2011. Characterization of mesoscale instabilities in localized granular

shear using digital image correlation. Acta Geotech. 6:205–217. doi:10.1007/s11440-011-0147-2

Romero, T., A. Gens, and A. Lloret. 2001. Temperature effect on the hydraulic behavior of an unsaturated clay. Geotech. Geol. Eng. 19:311–332. doi:10.1023/A:1013133809333

Rudnicki, J.W., and J.R. Rice. 1975. Conditions for the localization of deformation in pressure sensitive dilatant materials. J. Mech. Phys. Solids 23:371–394. doi:10.1016/0022-5096(75)90001-0

Salager, S., Jamin, F., M. Saïd El Youssoufi, and C. Saix. 2006. Influence of temperature on the water retention curve of porous media. C. R. Mec. 334:393–398. doi:10.1016/j.crme.2006.05.003

Salager, S., M. Rizzi, and L. Laloui. 2011. An innovative device for determining the soil water retention curve under high suction at different temperatures. Acta Geotech. 6:135–142. doi:10.1007/s11440-011-0141-8

Salager, S., M. Saïd El Youssoufi, and C. Saix. 2010. Definition and experimental determination of a soil-water retention surface. Can. Geotech. J. 47:609–622. doi:10.1139/T09-123

Schrefler, B.A. 1984. The finite element method in soil consolidation (with applications to surface subsidence). Ph.D. diss. Univ. College of Swansea, Swansea, Wales, UK.

Shan, Z., D. Ling, and H. Ding. 2012. Exact solutions for one-dimensional consolidation of single-layer unsaturated soil. Int. J. Numer. Anal. Methods Geomech. 36:708–722. doi:10.1002/nag.1026

Simo, J.C. 1992. Algorithms for static and dynamic multiplicative plasticity that preserve the classical return mapping schemes of the infinitesimal theory. Comput. Methods Appl. Mech. Eng. 99:61–112. doi:10.1016/0045-7825(92)90123-2

Song, X., and R.I. Borja. 2014. Mathematical framework for unsaturated flow in the finite deformation range. Int. J. Numer. Methods Eng. 97:658–682. doi:10.1002/nme.4605

Sugii, T., K. Yamada, and T. Kondou. 2002. Relationship between soil-water characteristic curve and void ratio. In: J.F.T. Juco et al., editors, Proceedings of the 3rd International Conference on Unsaturated Soils, Recife, Brazil. 10–13 Mar. 2002. Vol. 1. Swets and Zeitlinger, Rotterdam, the Netherlands. p. 209–214.

Sun, W., and D. Sun. 2012. Coupled modelling of hydro-mechanical behavior of unsaturated compacted expansive soils. Int. J. Numer. Anal. Methods Geomech. 36:1002–1022. doi:10.1002/nag.1036

Tamagnini, R. 2004. An extended Cam-clay model for unsaturated soils with hydraulic hysteresis. Geotechnique 54:223–228. doi:10.1680/geot.2004.54.3.223

Tang, A.M. 2005. Effect de la temperature sur le comportement des barrieres de confinement. Ph.D. diss. Ecole Nationale des Ponts et Chaussees, Paris.

Tarantino, A., and S. Tombolato. 2005. Coupling of hydraulic and mechanical behavior in unsaturated compacted clay. Geotechnique 55:307–317. doi:10.1680/geot.2005.55.4.307

Uzuoka, R., and R.I. Borja. 2012. Dynamics of unsaturated poroelastic solids at finite strain. Int. J. Numer. Anal. Methods Geomech. 36:1535–1573. doi:10.1002/nag.1061

van Genuchten, M.Th. 1980. A closed-form equation for predicting the hydraulic conductivity of unsaturated soils. Soil Sci. Soc. Am. J. 44:892–898. doi:10.2136/sssaj1980.03615995004400050002x

Wu, L.Z., L.M. Zhang, and R.Q. Huang. 2012. Analytical solution to 1D coupled water infiltration and deformation in two-layer unsaturated soils. Int. J. Numer. Anal. Methods Geomech. 36:798–816. doi:10.1002/nag.1044

Zha, Y., J. Yang, L. Shi, and X. Song. 2013. Simulating one-dimensional unsaturated flow in heterogeneous soils with water content-based Richards equation. Vadose Zone J. 12(2). doi:10.2136/vzj2012.0109

Zhang, Z.F. 2011. Soil water retention and relative permeability for conditions from oven-dry to full saturation. Vadose Zone J. 10:1299–1308. doi:10.2136/vzj2011.0019